1037
c.1

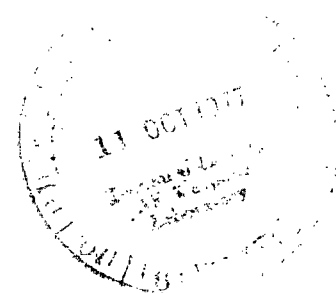NASA Technical Paper 1037

Mean Velocity, Turbulence Intensity, and Scale in a Subsonic Turbulent Jet Impinging Normal to a Large Flat Plate

Donald R. Boldman and Paul F. Brinich

SEPTEMBER 1977

NASA

NASA Technical Paper 1037

Mean Velocity, Turbulence Intensity, and Scale in a Subsonic Turbulent Jet Impinging Normal to a Large Flat Plate

Donald R. Boldman and Paul F. Brinich
Lewis Research Center
Cleveland, Ohio

MEAN VELOCITY, TURBULENCE INTENSITY, AND SCALE IN A
SUBSONIC TURBULENT JET IMPINGING NORMAL TO A
LARGE FLAT PLATE

by Donald R. Boldman and Paul F. Brinich

Lewis Research Center

SUMMARY

Mean velocity, turbulence intensity, and scale were measured in a subsonic turbulent jet impinging normal to a large flat plate in order to explain the increase in noise associated with the impinging flow. The apparatus was similar to a configuration previously used in jet impingement noise studies. The measurements were taken at nominal jet velocities of 61, 138, and 192 meters per second with the plate located 7.1 nozzle-exit diameters from the nozzle.

The maximum turbulence intensity at the locus of the plate was approximately the same with or without the plate; however, the integral length scale, inferred from spectra, was generally less with the plate than with the free jet. The measured intensities and length scales, in conjunction with a contemporary theory of aerodynamic noise, provided a good explanation for the observed increase in noise associated with jet impingement. An increase in the volume of highly turbulent flow could be a principal reason for the increase in noise.

INTRODUCTION

It has long been recognized that an increase in noise occurs when large surfaces such as aircraft flaps and thrust reversers are inserted into a jet. The increase in noise resulting from the edge effects on these surfaces is reasonably well understood; however, the increase in noise associated with the main surface of the body, often called scrubbing or impingement noise, has not been explained. The present study is directed toward this goal.

This investigation supplements the study described in reference 1, in which an appreciable increase in noise was observed in an impinging jet relative to that from a free

jet operating at the same velocity. A comprehensive theoretical study of this problem in reference 2 suggested that the observed increase in noise might be explained by a difference in the turbulence structure between free and impinging jets. In the present study, some of these differences are assessed, with emphasis on the differences in integral length scale and turbulence intensity in the mean flow direction.

Studies of the impingement of a turbulent jet on a solid boundary have been rather numerous in the last decade, principally because of the prevalence of this type of flow in aerospace applications. In many studies, the primary objective was to analyze the pressure and velocity fields (refs. 3 to 8) and the heat transfer (ref. 9). Although turbulence measurements have been made in impinging flow (e. g., refs. 10 to 12), the results have not been sufficient to explain the role of turbulence in noise generation. In the present study the nozzle and plate configuration was similar to that used in the noise study in reference 1 in that the dimensions of the nozzle and the plate were identical in both experiments. The turbulence associated with the impinging flow in the present study should then be the same as the turbulence associated with the noise data reported in reference 1.

SYMBOLS

c_0 ambient speed of sound

D nozzle diameter

F normalized power spectrum function defined by eq. (5)

f frequency

k wave number

L integral length scale

M_c convection Mach number of sound sources

P_s static pressure

P_0 stagnation pressure

PWL_T total sound power level, dB

$\mathscr{P}$ sound power

R free jet half-radius (radius at which velocity is one-half its maximum value at a distance corresponding to plane of plate)

Re_D Reynolds number based on nozzle diameter

$\mathscr{R}$ gas constant

r	coordinate denoting distance in radial direction
T_0	stagnation temperature
V	magnitude of mean velocity vector
V_c	mean velocity along jet centerline
V_N	mean velocity at nozzle exit
V'_s	overall root-mean-square (rms) component of velocity in streamwise direction of mean flow
v	incremental volume of jet
v'_s	root-mean-square (rms) component of velocity in a frequency band
Z	coordinate denoting axial distance from nozzle exit
z	coordinate denoting distance from plate
α	eddy viscosity
β	effective bandpass width
γ	ratio of specific heats
λ	wavelength
ρ_0	ambient density
φ	sound power spectral density

Subscripts:

| free | condition in a free jet |
| imp | condition in an impinging jet |

APPARATUS

A vertical free jet, flowing downward, impinged upon a large flat plate mounted horizontally, as shown in figure 1. The apparatus was similar to that used in the noise study in reference 1, except that, in the noise study, the plate was mounted vertically. A 0.61-meter-inside-diameter by 1.22-meter-long plenum was supported from the ceiling and connected to a high-pressure air supply. The plenum contained a series of screens and flow straighteners as well as filters that removed much of the fine dust (iron oxide) from the airstream. The dust, which is often present in the supply lines of high-pressure air systems, can cause premature failure of sensitive instruments such as hot wires immersed in high-velocity streams. The installation of two 0.6-centimeter-thick felt dust filters permitted satisfactory operation with fine tungsten

3

hot wires at velocities as high as 192 meters per second; in the absence of the filters, velocities had to be limited to about 90 meters per second.

An elliptically contoured, circular nozzle with an exit diameter of 5.21 centimeters and a lip thickness of 0.86 centimeter was connected to the plenum. Turbulence measurements were made at exit velocities of 61, 138, and 192 meters per second. The highest velocity (192 m/sec) represents the operating condition in which the noise measurements reported in reference 1 were made. The desired velocity level was set by means of two pneumatic valves located about 3.9 meters upstream of the plenum. These valves were arranged with the smaller valve forming a bypass circuit around the larger valve.

The 2.4-meter-square wooden plate used in the impingement tests was covered with a plastic-laminate surface. This plate was supported on the underside by a steel channel framework that was attached to four cornerposts, as shown in figure 1. A 7.6-centimeter-wide sliding strip passed along the center of the plate. This "slider" supported a motorized actuator that was used to position a hot-wire probe in the direction of the z-axis, as shown in figure 2. The slider and probe actuator assembly was manually translated in the radial direction (denoted by the coordinate r in fig. 2) and clamped in position. The hot-wire probe could therefore be located at any point in the Z,r plane (or z,r plane) so that regions of maximum turbulence could be readily determined. By attaching the actuator underneath the plate, only the hot-wire probe was immersed in the impinging flow, thus minimizing the disturbance to the flow field. During the jet impingement tests the plate was located 37.1 centimeters from the nozzle exit (fig. 2) and normal to the axis of the jet. The flow direction resulting from this arrangement of the nozzle and plate is often referred to as normal impingement.

MEASUREMENTS

Nozzle-exit velocities were determined simply by measuring the pressure and temperature of the air in the plenum and the nozzle-exit static pressure, which was assumed to be equal to the ambient pressure of the test cell. A pitot-pressure probe and a Chromel-Alumel temperature probe located near the centerline of the plenum provided the stagnation pressure P_0 and temperature T_0, respectively. These quantities, along with the static pressure P_s, describe the nozzle-exit velocity according to the relation

$$V_N^2 = \frac{2\gamma \mathscr{R} T_0}{\gamma - 1}\left[1 - \left(\frac{P_s}{P_0}\right)^{(\gamma-1)/\gamma}\right]$$

(1)

which is valid for an isentropic, perfect gas (ref. 13). The ratio of specific heats γ is 1.4 for air at room temperature.

Mean velocities were measured in the free jet with a pitot pressure probe and with hot wires. In the impinging flow, only the hot wires were used to measure velocity. Using a pressure sensing probe to measure the velocity in an impinging flow becomes more difficult since the constant-static-pressure assumption, valid for free jets, is no longer applicable. Also, it would be necessary to use a directionally sensitive probe because of the streamline curvature. A single hot wire oriented normal to the streamline senses the speed in the streamwise direction, which is indicated by the subscript s; however, the flow direction cannot be determined.

The pitot pressure probe used in the free-jet velocity surveys had an outside tip diameter of about 0.1 centimeter. This probe was driven by a motorized actuator connected to a vertical support that rested on the test plate and was located 60 centimeters from the nozzle centerline. The probe was traversed in the horizontal plane by commencing at the vertical centerline of the jet and retracting the probe radially toward the actuator. The vertical centerline was established by lowering a plumb bob from the center of the nozzle. This same method was used in making the hot-wire measurements in the free jet.

The hot-wire measuring system is depicted schematically in figure 3. The signal from a 0.0005-centimeter-diameter, tungsten hot-wire probe and a constant-temperature anemometer was fed to a signal conditioner and an oscilloscope. The signal was linearized (i.e., the output potential was a linear function of mean velocity) and monitored on a direct-current (dc) voltmeter and true root-mean-square (rms) meter.

The linearized signal of mean velocity was plotted as a function of position on an XY recorder. Signals at various points in the flow field were simultaneously recorded on two channels of a magnetic tape recorder. One of the channels was frequency modulated (FM) with a frequency response from dc to 20 kilohertz, flat to within ±0.5 decibel. The other channel operated in a direct-record mode with a frequency response of 150 hertz to 150 kilohertz, flat to within ±3.0 decibels. The direct-record mode was used in order to attain a high-frequency response at reasonable tape speeds (76 cm/sec). Taped signals 2 to 3 minutes in duration were analyzed with a narrow-band spectrum analyzer having an effective bandpass width β of 6 hertz.

The hot wire was calibrated prior to each test condition (data at a given nozzle-exit velocity) by placing it at the center of the nozzle exit. Nonlinear distortion of the signal was less than 5 percent of the mean velocity at velocities to about 138 meters per second. At higher velocities the signal was curve fitted with a second-order polynomial to account for the nonlinearity of the output.

A few tests were performed with a microphone placed just outside the free jet in the plane of the plate. These tests were conducted with a 0.32-centimeter-diameter condenser microphone coupled to an amplifier and a magnetic tape recorder. The mi-

crophone frequency response was essentially flat to 50 kilohertz, thus permitting sound measurements appreciably outside the audible range.

RESULTS

Mean Velocity Distributions

Free jet. - Free-jet mean velocity surveys were made along the centerline $(r = 0)$ of the jet and along radii in the plane $z = 0$ corresponding to the plane of the plate in the case of the impinging jet $(Z = 37.1 \text{ cm})$. These measurements were made for two reasons. First, determining whether the present results were consistent with documented results for free jets (refs. 4, 12, 14, and 15) would provide confidence in the instrumentation and flow systems. Second, it was necessary to establish a set of reference conditions for the present study. This required surveys in a specific plane of the free jet, namely, the plane where the plate would be located.

Centerline velocities at three axial stations are plotted as a function of nozzle-exit velocity in figure 4. At the position closest to the nozzle $(Z/D = 3.90)$, the presence of the potential core is evident since the core and nozzle-exit velocities are equal (i. e., $V_c/V_N = 1.0$). However, in the plane where the plate would be located $(Z/D = 7.12)$, the centerline velocity dropped to about 90 percent of the nozzle-exit velocity. The results in figure 4 suggest that at the lowest nozzle-exit velocities, the velocity ratio V_c/V_N was affected by the size of the valve used to control the flow. At nozzle-exit velocities below 140 meters per second, lower centerline velocities were obtained when the flow was controlled with the smaller valve (bypass valve) in the system. At nozzle-exit velocities above 140 meters per second, the velocity ratios were approximately equal.

The anomaly concerning the differences in centerline velocities arising from differences in the size of the flow control valve has not been resolved. Hot-wire measurements of centerline velocity were consistent with the pitot tube results; that is, higher velocities were indicated when the large valve was used to set the flow (for the same values of stagnation pressure measured in the plenum). The hot-wire measurements of rms velocity V_s' were nearly the same; therefore, since the mean velocity was higher when the large valve was used, the turbulence intensity V_s'/V_c was proportionally lower. This result suggests that the valves were affecting the turbulence differently and that the plenum may not have completely suppressed these differences. The greatest influence of the valves on the mean velocity measurements was noted at a Z/D of 7.12, which is near the end of the potential core.

In the following results, the flow was controlled by only the small valve at the lowest nozzle-exit velocity (61 m/sec). The small valve provided better control of the flow

at low velocities. At the higher nozzle-exit velocities (138 and 192 m/sec), the large valve was used to control the flow and the small one was used only for minor adjustments.

The slight increase in centerline velocity with increasing nozzle-exit velocity (fig. 4) is the result of an increase in the length of the core region. In reference 14 it was shown that downstream of the core the velocity ratio V_c/V_N can be expressed as a function of the axial distance Z/D and the Reynolds number by

$$\frac{V_c}{V_N} = 2.13 \ Re_D^{0.097} \left(\frac{Z}{D}\right)^{-1} \tag{2}$$

Velocity ratios calculated from this equation show a greater dependence on V_N than indicated by the present results. This is shown in figure 4 for a Z/D of 9.76.

In figure 5 the centerline velocity ratio is shown as a function of axial distance from the nozzle exit. The distributions are for a nozzle-exit velocity of 138 meters per second, which was sufficiently high to preclude the influence of the control valve system. The results for the free jet compare favorably with the data of several investigators as given in reference 14. In much of the reported data, velocity ratios, were measured at far greater values of Z/D than are pertinent to the present study; these velocity ratios were shown to vary inversely as a function of Z/D.

In figure 6 the local mean velocity distribution $V(r)$ is plotted for the three nozzle-exit velocities (61, 138, and 192 m/sec) at a Z/D of 7.12, which corresponds to the plane of the plate. The velocity profiles measured with the pitot tube are essentially independent of the nozzle-exit velocity, as would be expected since the Reynolds number is high ($2 \times 10^5 \leq Re_D \leq 6.5 \times 10^5$). The data from the pitot tube are in good agreement with the results based on hot-wire measurements. These data are also consistent with predictions based on the solution to the equation of mean motion for a circular jet given in reference 15, which can be written as

$$\frac{V}{V_c} = 0.048 \ \alpha^{-1/2} \left[1 + \frac{\left(\frac{r}{Z}\right)^2}{8\alpha}\right]^{-2} \tag{3}$$

where α represents the eddy viscosity. The centerline velocity V_c was related to the nozzle-exit velocity V_N by the following empirical expression given in reference 15:

$$V_c = 6.39 \, V_N \left(\frac{Z}{D}\right)^{-1} \tag{4}$$

The constant α in equation (3) was assumed to have a value of 0.00196, which was the value used in reference 16 to describe the velocity profiles at Z/D greater than 10.

The good agreement between the experimental data of this study and the theoretical mean velocity profile suggests that the profile has become essentially self-preserving at a distance of 7.12 nozzle-exit diameters. Townsend (ref. 15) states that a self-preserving form of the mean velocity profile can occur at distances greater than 8 diameters; therefore, the agreement between profiles shown in figure 6 is not surprising.

The data in figure 6 were used to define a reference length R that represents the radius of the jet for which the velocity ratio is 0.5. This reference length, called the half-radius of the free jet in the plane of impingement, was used to nondimensionalize the spectral data presented later. Accordingly, the value of R, based on the pitot tube measurements of velocity, is 3.6 centimeters.

Impinging flow. - The axial distribution of mean velocity in the impinging flow is shown in figure 7 for the intermediate nozzle-exit velocity (138 m/sec). The mean velocities in the impinging jet do not depart from the values in the free jet for approximately 5 nozzle diameters. Thereafter, a pronounced reduction in the velocity of the impinging jet can be observed, as was also noted in references 6 and 12 for comparable spacing between the plate and the nozzle. In reference 12 this characteristic behavior, in conjunction with centerline turbulence measurements, suggested the absence of serious lateral oscillations (flapping) of the jet. Such oscillations could have significantly altered the turbulence characteristics of the impinging jet. Likewise, in the present study, jet flapping could compromise the turbulence data in the impinging flow. However, since the axial distributions of mean velocity in the free and impinging jets are essentially the same as the results presented in references 6 and 12, the jet flapping effects were probably negligible.

Distributions of mean velocity in the impingement zone are presented as a function of the distance from the plate for various radial positions and nozzle-exit velocities in figure 8. Along the centerline of the jet ($r = 0$), the velocity decays from a value close to the nozzle-exit velocity to a value that approaches zero at the plate. At radial positions ranging from 2.5 to 10.2 centimeters, the velocity reaches a peak value very close to the wall. In the present study the hot wire was traversed to within 0.1 centimeter of the wall. This was not sufficiently close to define the peak in the velocity profile at the lowest nozzle-exit velocity (61 m/sec, (fig. 8(a)). However, as the nozzle-exit velocity was increased to 138 meters per second and finally to 192 meters per second, the peak in the velocity profiles became more apparent, as shown in figures 8(b) and (c). Thus, the peak velocity was displaced outward from the surface as the nozzle-exit velocity

was increased.

The lowest nozzle-exit velocity in the present study (61 m/sec) was nearly twice as high as the nozzle-exit velocity for the impinging flow study described in reference 6. However, it is interesting to compare the mean velocity results because of the geometric similarity of the two configurations. In reference 6 it was observed that the peak velocity occurred near the wall in the impingement zone. According to the pressure data of reference 6, the impingement zone, defined as the zone in which the static pressure exceeds the ambient pressure, was relatively small. If the results in reference 6 are interpolated to account for the slightly different dimensionless distance between the plate and the nozzle, the boundary between the impingement zone and the wall-jet region would be about 3 nozzle diameters from the centerline (~15 cm). In figure 8, the profile at an r of 10.2 centimeters would lie within the impingement zone; the profiles at r of 20.3, 40.6, and 91.4 centimeters presumably lie in the wall-jet region in which the static pressure is equal to the ambient pressure.

The radial variation of peak velocity is compared with the data in reference 6 in figure 9. The agreement is very good at the lowest nozzle-exit velocity (61 m/sec), which is closest to the velocity used in the study of reference 6. (The peak velocity was assumed to be the maximum measured velocity near the wall when a peak value was not clearly defined.) At higher nozzle-exit velocities the peak velocities in the radial direction tend to become higher. This trend was expected because higher nozzle-exit velocities tend to lengthen the core region in the jet. The effect of a longer core region resulting from an increase in the jet Reynolds number (or nozzle-exit velocity) can be interpreted as the effect of decreasing the dimensionless distance between the nozzle and the plate at a fixed nozzle-exit velocity. Results for this latter case, presented in reference 8, show that the peak radial velocity increases with decreasing dimensionless nozzle-to-plate spacing, a consistent trend in the results.

Contours of constant mean velocity in the impinging jet are shown in figure 10 for a nozzle-exit velocity of 138 meters per second. These contours were obtained by interpolating the data in figure 8(b) for the region defined by $0 < z < 8$ centimeters. The free-jet data in reference 17 were used to extrapolate the present data to the vicinity of the nozzle exit. The radial locations where hot-wire traverses were made are also presented for radial positions to 20.3 centimeters. These contours indicate that a rapid reduction in velocity occurs in a very narrow region about the stagnation point on the plate. As the jet sweeps radially outward, much of the high-velocity air is contained in the region close to the wall.

In the previous discussion of the mean velocity distributions in the impinging jet, deviation from the free-jet centerline velocity occurred at about 2.1 nozzle diameters from the plate. This represents the location of the upper boundary of the impingement region. In the radial direction, the boundary between the impingement region and the wall-jet region was estimated to be about 3 nozzle diameters from the center of the jet

(ref. 6). These boundaries are shown in figure 10; and the free-jet, impinging jet, and wall-jet regions are identified.

Turbulence Intensity

Free jet. - The turbulence intensity distributions for the free jet in the plane corresponding to the plate location are shown in figure 11. In the outer portion of the profiles (R > 4 cm), there is a consistent trend of decreasing turbulence intensity with increasing velocity (or Reynolds number). This same Reynolds number effect on the turbulence has been observed elsewhere (e.g., ref. 17). However, at the centerline, the turbulence intensities differed in a random fashion, with the lowest intensity occurring at the intermediate velocity of 138 meters per second. In repeated tests the centerline values of turbulence intensity differed slightly, indicating randomness of the flow near the tip of the potential core (ref. 14).

The feature of primary interest in the present study is the maximum turbulence intensity, which occurs at a radius of about 2.5 centimeters or slightly greater. This is essentially along the centerline of the mixing layer, which is a line parallel to the jet axis at the radius of the nozzle lip. The maximum turbulence intensity V_s'/V_N has a nominal value of 0.15, consistent with the values reported in references 4 and 17 for similar free-jet flows. In the following section, these maximum turbulence intensities are compared with the maximum intensities obtained in the impinging flow.

Impinging flow. - Turbulence intensities were obtained in conjunction with all of the mean velocity measurements presented in figure 8; however, the highest levels of intensity are of primary interest in this study because of the strong influence of the turbulence intensity on noise production. As a result of extensive turbulence surveys in the z, r plane of the impinging flow, the highest levels of turbulence were observed at two radial locations in a region very close to the centerline of the mixing region for the free jet. These radial stations were located at r of 2.5 and 3.8 centimeters. Distributions of the turbulence intensity V_s'/V_N at these positions are presented in figure 12 for nozzle-exit velocities of 61, 138, and 192 meters per second. Turbulence intensity distributions at the other radial positions (r of 0, 5.1, 10.2, 20.3, 40.6, and 91.4 cm) are also presented for the intermediate nozzle-exit velocity (of 138 m/sec) in figure 12(b). These latter results are essentially typical of the turbulence intensity distributions for the other nozzle-exit velocities. To get a better picture of the turbulence field, contours of constant turbulence intensity were developed from the results in figure 12(b) and are presented in figure 13.

In figures 12 and 13, in general, the highest levels of turbulence intensity were measured along the centerline of the free-jet mixing layer (r = 2.5 cm) at each nozzle-exit velocity. The turbulence intensity was nearly constant in the vertical direction from

the plate. At the highest nozzle-exit velocity (192 m/sec), the turbulence intensity levels were quite high near the wall, with V'_s/V_N approaching 0.25 (fig. 12(c)). Outside this near-wall region the level of turbulence intensity diminished rapidly to the levels measured at the lower nozzle-exit velocities. Over most of the region of maximum turbulence, the intensity was equal to or only slightly higher than the maximum levels obtained in the free jet. These maximum levels of turbulence intensity ranged from 0.16 to 0.17 (except very near the wall for a V_N of 192 m/sec), as compared with a nominal value of 0.15 for the free jet. However, these maximum levels were present only in a very small region of the jet, as shown in figure 13. The data in reference 11 revealed that the maximum turbulence levels in the region near the plate were not larger than the turbulence in the approach jet.

The present tests suggest that the maximum levels for the free jet and impinging flow might differ by only about 10 percent in a very small region, with the turbulence in the impinging flow being slightly higher. (Again this excludes the very narrow region near the wall, where intensities approaching 0.25 were observed at the highest nozzle-exit velocity of 192 m/sec.)

Spectra and Scale of Turbulence

The one-dimensional turbulence spectra of V'^2_s are presented in terms of a normalized power spectrum based on a nondimensional frequency Rk, where the wave number k equals $2\pi f/V$. The normalized power spectrum can be written as

$$F(Rk) = \frac{V}{2\pi R\beta} \frac{v'^2_s(Rk, \beta)}{V'^2_s} \tag{5}$$

where v'^2_s is the mean square of the velocity fluctuations in the bandpass width β. The normalized power spectral density satisfies

$$\int_j^\circ F(Rk)d(Rk) = 1.0 \tag{6}$$

An integral length scale of the turbulence (refs. 12 and 17) is given by

$$L = \frac{\pi}{2} R\ F(0) \tag{7}$$

11

where the zero intercept of the spectrum function $F(0)$ is estimated from the value of F at the lowest frequency of the measurements. In the present study the lowest frequency for the spectra was 20 hertz. The reference length R was equal to the half-radius of the free jet in the plane of the plate (3.6 cm).

Free jet. - Spectra of $V_s'^2$ are presented for the free jet at two positions in the plane of the plate, namely, the centerline (fig. 14) and at the location of maximum turbulence intensity (fig. 15), which was nominally 2.5 centimeters from the centerline. At these positions the nozzle-exit velocity had a slight effect on the level of the spectral distributions in the low-frequency range, $Rk < 1.0$. At higher frequencies the characteristic -5/3 power falloff can be seen. This variation in the power spectra is typical of high-Reynolds-number turbulent flows (refs. 12 and 18).

A spike appears in the falloff region of the spectrum function at the higher nozzle-exit velocities. This spike is most pronounced at the highest nozzle-exit velocity (192 m/sec) and is least evident at the lowest nozzle-exit velocity (61 m/sec). The frequency of this signal is nominally 20 000 hertz. Similar spikes have been observed in the spectra of free jets (ref. 17) and impinging jets (ref. 5). In both cases, the high-amplitude signals were attributed to sound waves emanating from the jet. To determine whether the high-frequency spike in the turbulence spectra in this study was caused by a sound wave, narrow-band sound spectra were obtained just outside the mixing region in the plane of the plate. The distributions of sound power spectral density φ as a function of frequency are presented in figure 16. Although spikes are present at low frequencies ($f < 2500$ Hz), the spectrum does not have a spike near 20 000 hertz. This suggests that a high-frequency sound wave was not producing the spike in the turbulence spectra. Therefore, the spike in the turbulence spectra was probably associated with spurious signals from the hot-wire probe. Such signals can arise from a number of sources, including eddy shedding from the probe or wire supports, vibrations, and the wire acting as a strain gage (ref. 19).

From the $V_s'^2$ spectra just presented, estimates of the integral length scale L can be made with the aid of equation (7). If the zero intercept of the spectra is estimated to be about 0.4 for the three velocities, the length scale L would be equal to $0.4(\pi/2)R$, or 62 percent of the half-radius of the free jet ($R = 3.6$ cm). This result agrees with the length scale reported in reference 12. This free-jet length scale is compared with the length scale inferred from spectra in the impinging jet in the following section.

Impinging flow. - Spectral densities were determined at two locations in the impinging jet in the regions of highest turbulence intensity. These positions can be identified in the z, r plane as (3.3, 2.5) and (0.1, 3.8), where the distances are given in centimeters. The spectral density distributions are presented in figure 17 for each of the three nozzle-exit velocities. As in the free jet, all distributions exhibit the -5/3 power falloff at nondimensional frequencies above 1.0. The low-frequency spectra are gener-

ally flat and therefore can be extrapolated to provide values of $F(0)$ from which an integral length scale can be estimated. The spectra in figure 17 show that the length scales are essentially the same at the two positions. Most of the data suggest a length scale in the regions of maximum turbulence of about 35 percent of the free-jet half-radius. This is based on an average of the data in the flat portion of the spectra in the region $Rk < 1.0$.

To determine the variation in the length scale in the impingement zone, low-frequency $V_s'^2$ spectra were obtained at several points along a normal path defined by $z, 2.5$ and along a horizontal path defined by $0.1, r$. The results of these tests, which were performed at the intermediate nozzle-exit velocity (138 m/sec), are presented in figure 18.

All spectra along the path $z, 2.5$ exhibited a well-defined flat region from which values of $F(0)$ could readily be determined (fig. 18(a)). Length scales based on these spectral densities tended to drop slightly and then increased as the distance from the plate was increased. In progressing radially outward along the path $0.1, r$, the integral length scale was nearly constant for radial distances to about 20 centimeters (fig. 18(b)). These data tend to be distributed about a line at $F(Rk) \approx 0.2$.

The length scales estimated from the data in figure 18 are plotted as a function of axial and radial distances in figures 19 and 20, respectively. The mean velocity distribution along the path in which the measurements were obtained is also presented in these figures. Generally, the local mean velocity was appreciably lower than the nozzle-exit velocity (138 m/sec) in the region of the measurements.

The length scales previously measured for the free jet are presented in figures 19 and 20 as a reference level for comparison with the impinging flow results. It is clear from these figures that integral length scales are definitely smaller in the impingement zone than in the free jet. In figure 19, the value of L obtained at the center of the mixing zone is extrapolated linearly in the upstream direction (direction of increasing z) to zero at the nozzle lip. The length scale in the impinging flow tends to approach the estimated value of L for the free jet, as would be expected.

DISCUSSION OF RESULTS

In the experiments reported in references 1 and 20 a significant increase in radiated acoustic power was observed when a large plate was inserted in a free jet. Both studies revealed that the acoustic power output of the impinging jet varies approximately as the eighth power of velocity V_N^8, which indicates a quadrupole noise source. Data made available by the authors of reference 1 have been used to generate curves of the total sound level as a function of nozzle-exit velocity after applying corrections for ground reflections. (These corrections were not included in the results presented in ref. 1.)

The dependence of total sound power level PWL_T on nozzle-exit velocity V_N for the jet alone and for the impinging jet are shown in figure 21. Eighth-power curves with and without the effects of convection of the sound sources by the mean flow (ref. 21) are shown for comparison with the data. Convection resulted in upward curvature of the function $PWL_T(V_N)$ at high nozzle-exit velocities. It is clear from figure 21 that the eighth-power (quadrupole source) representation of sound power is reasonably good to a velocity of about 300 meters per second. An increase in PWL_T of about 4 decibels occurs when the impingement plate obstructs the free jet. This change in sound power level (ratio of impinging jet power to free-jet power) is nearly independent of nozzle-exit velocity.

The plate can produce changes in the radiated sound power by (1) changing the acoustic impedance experienced by the sources, (2) changing the source structure, and (3) changing the convective amplification of the sound by altering the source velocity. Changes in acoustic impedance can arise directly through the presence of the plate and indirectly through changes in the mean flow field caused by the plate. Changes in source structure arise primarily through (1) changes in turbulence intensity, (2) changes in length scale, and (3) changes in the volume of intense turbulence. Evidence of changes in source structure has already been presented. The changes in convective amplification can be interpreted as a kind of acoustic impedance change.

It is difficult to assess the influence of convective amplification. In a free jet, it is given by $\left(1 + M_c^2\right)\Big/\left(1 - M_c^2\right)^4$ (ref. 2), where M_c is the convection Mach number of the sources. The sources in the impinging jet are moving in different directions in each region of the jet rather than in a single direction, and it is not clear what the amplification factor will be in this case. However, it is believed that the differences in convective amplification resulting from the redirection of the sources in the presence of the plate will be small.

If it is assumed that convective amplification as well as flow impedance effects can be neglected, the contribution of the source modification to the acoustic power change can be approximated by considering the following equation for the sound power per unit volume of free turbulence derived in reference 2 (p. 180) and expressed in the present nomenclature:

$$\frac{\mathscr{P}}{\text{Unit volume}} \propto \frac{\rho_0 \left(\frac{V_s'}{V_N}\right)^8 V_N^8}{c_0^5 L} \tag{8}$$

The analysis in reference 22 shows that this expression should also apply to the turbulence in the vicinity of a large plate, provided it is multiplied by a factor of 2 for source

regions within about a wavelength of the plate. This factor accounts for the direct acoustic impedance change due to the presence of the plate. In addition to this direct acoustic impedance contribution, the increase in noise could result from an increase in turbulence intensity, a decrease in length scale, a change in the volume of intense turbulence, or a combination of these factors.

The total power radiated by the jet can be obtained by summing equation (8) over all incremental volumes containing significant turbulence intensity in order to obtain the ratio of power radiated in the impinging jet to power radiated by the free jet.

$$\frac{\mathscr{P}_{imp}}{\mathscr{P}_{free}} \approx \frac{\displaystyle\sum_{n=1}^{m_1} \frac{v_{n,imp}\left(\dfrac{V'_s}{V_N}\right)^8_{n,imp}}{L_{n,imp}} + \displaystyle\sum_{n=m_1}^{m} \frac{2v_{n,imp}\left(\dfrac{V'_s}{V_N}\right)^8_{n,imp}}{L_{n,imp}}}{\displaystyle\sum_{n=1}^{m} \frac{v_{n,free}\left(\dfrac{V'_s}{V_N}\right)^8_{n,free}}{L_{n,free}}} \tag{9}$$

where v_n represents an incremental volume in the flow field. This result depends not on the nozzle-exit velocity but rather on the turbulence intensity, which is relatively independent of nozzle-exit velocity. The change in radiated power level, in decibels, can be expressed as

$$\Delta PWL_T = 10 \log_{10} \frac{\mathscr{P}_{imp}}{\mathscr{P}_{free}} \tag{10}$$

In equation (9) the terms in the numerator are summed over the volume of flow from the nozzle exit to an outer boundary located at an r of 20.3 centimeters. This is slightly beyond the radial boundary of the impingement zone; however, fairly high levels

of turbulence intensity are still present at this station (figs. 12(b) and 13). Also, length scales in this region are small compared with those for a free jet (fig. 20). The second term in the numerator accounts for the doubling of power due to direct acoustic impedance changes caused by the presence of the board and was assumed to be applicable to the region within 8 centimeters of the board (approximately a half-wavelength based on a peak frequency of 2000 Hz (ref. 1)).

The denominator in equation (9) represents an equal volume of flow in the free jet. In this case, the region of interest extends to about 10.7 nozzle-exit diameters from the nozzle (fig. 22).

Length scales in the impinging jet were estimated from the results shown in figures 19 and 20. The turbulence intensity was estimated from the results shown in figure 13. The values of turbulence intensity and length scales in the free jet were obtained from the data in reference 17. Since the radiated sound power varies as the eighth power of turbulence intensity, it is obvious that regions of low turbulence intensity contribute negligibly to the total radiated power (e.g., the potential core and outer regions of the jet).

The contributions to the radiated power from various portions of the free and impinging jets are shown in figure 22. These results were normalized to the contribution from the free-jet mixing zone extending 5 nozzle-exit diameters from the nozzle. This region was the same for both jets. In the impinging jet the largest contribution to the total radiated sound came from the impingement zone (region nearest the plate). Since the maximum turbulence intensities in the free and impinging jets were about the same, the results in figure 22 imply that the principal reason for the increase in radiated noise in the impinging jet was a larger volume of highly turbulent flow. The reduced length scale in the impingement region, as well as the direct change in acoustic impedance by the plate, also accounted for some of the increase in radiated sound power (eq. (8)).

Summation of the values of sound power in figure 22 in conjunction with equation (10) yields the following estimate of the increase in total sound power level based on the volume-weighting technique:

$$\Delta PWL_T = 10 \log_{10} \frac{\mathscr{P}_{imp}}{\mathscr{P}_{free}} = 10 \log_{10} \frac{4.01}{1.59} = 4.0 \text{ dB}$$

This change in estimated sound power is in very good agreement with the results of reference 1, presented in figure 21.

As mentioned earlier, changes in acoustic power due to changes in the mean flow and convective amplification could not be estimated. However, the good agreement between the estimated and experimental changes in total sound power level suggest that these factors either cancel each other or are both small - the latter being the more probable explanation.

SUMMARY OF RESULTS

Mean velocity, turbulence intensity, and integral scale were measured in a sub-sonic turbulent jet impinging normal to a large flat plate. These measurements were obtained with a specific nozzle and plate configuration, which was a full-scale facsimile of the apparatus used in another investigation of the far-field noise. The tests were performed in free and impinging jets at nominal nozzle-exit velocities of 61, 138, and 192 meters per second. In the impinging flow tests, the plate was located 7.1 nozzle-exit diameters from the nozzle. The data from this study were used in conjunction with theory to provide a possible explanation for the observed increase in sound power emanating from the impinging jet relative to free-jet noise. The results of this investigation can be summarized as follows:

1. Spectral measurements at the points of maximum turbulence intensity in both the free and impinging jets revealed, in all cases, the classical -5/3 power falloff in the spectra. Integral length scales, inferred from the spectra, decreased from the free-jet value at about 2 nozzle diameters from the plate to one-half this value near the plate. Radial distributions of length scale in the impingement zone near the wall revealed that the scale was nearly constant within 4 diameters of the jet centerline.

2. The maximum turbulence intensity was about the same in the impingement region as in the free jet. The rms velocity component was nominally 15 percent of the nozzle-exit velocity. Very close to the surface the turbulence intensity exceeded 20 percent, but only at the highest nozzle-exit velocity of 192 meters per second. In general, highest turbulence intensity was observed at two zones in the impingement zone. One zone was along the centerline of the mixing region about 0.5 nozzle diameter from the plate, and the other point was near the wall at a distance of about 0.7 diameter from the jet centerline.

3. Measurements of turbulence intensity and length scale were incorporated in a contemporary theory for aeroacoustic noise in order to predict the increase in radiated acoustic power that was observed by others when a large plate was inserted in a free jet. The calculated increase in radiated acoustic power was in good agreement with the experimental results. The increase in noise appeared to be largely due to a greater volume of high turbulence in the impinging jet relative to the free jet. The reduced length scale, as well as direct changes in acoustic impedance due to the presence of the plate, also accounted for part of the increase in radiated acoustic power.

Lewis Research Center,
   National Aeronautics and Space Administration,
      Cleveland, Ohio, May 23, 1977,
         505-03.

REFERENCES

1. Olsen, William A.; Miles, Jeffrey H.; and Dorsch, Robert G.: Noise Generated by Impingement of a Jet upon a Large Flat Board. NASA TN D-7075, 1972.

2. Goldstein, Marvin E.: Aeroacoustics. McGraw-Hill, Inc., 1976.

3. Wolfshtein, M.: Some Solutions of the Plane Turbulent Impinging Jet. J. Basic Eng., vol. 92, ser. D, no. 4, Dec. 1970, pp. 915-922.

4. Bradshaw, P.; and Love, Edna M.: The Normal Impingement of a Circular Air Jet on a Flat Surface. R. & M. No. 3205, British A.R.C., 1959.

5. Wagner, F. R.: The Sound and Flow Field of an Axially Symmetric Free Jet upon Impact on a Wall. NASA TT F-13,942, 1971.

6. Tani, I.; and Komatsu, Y.: Impingement of a Round Jet on a Flat Surface. Applied Mechanics; Proceedings of the Eleventh International Congress of Applied Mechanics, Munich (Germany) 1964, Henry Görther, ed., Springer-Verlag, 1966, pp. 672-676.

7. Bradbury, L. J. S.: The Impact of an Axisymmetric Jet onto a Normal Ground. Aeronautical Quarterly, vol. 23, pt. 2, May 1972, pp. 141-147.

8. Hrycak, Peter; et al.: Experimental Flow Characteristics of a Single Turbulent Jet Impinging on a Flat Plate. NASA TN D-5690, 1970.

9. Donaldson, Coleman Dup.; and Snedeker, Richard S.: A Study of Free Jet Impingement. Part I. Mean Properties of Free and Impinging Jets. J. Fluid Mech., vol. 45, pt. 2, Jan. 1971, pp. 281-319.

10. Chao, J. L.; and Sandborn, V. A.: Evaluation of the Momentum Equation for a Turbulent Wall Jet. J. Fluid Mech., vol. 26, pt. 4, Dec. 1966, pp. 819-828.

11. Foss, John F.: Measurements in a Large Angle Oblique Jet Impingement Flow. (Third Year Tech. Rept., Part 1, Michigan State Univ.; NASA Grant NGR 23-004-091.) NASA CR-138467, 1971.

12. Donaldson, Coleman Dup.; Snedeker, Richard S.; and Margolis, David P.: A Study of Free Jet Impingement. Part 2. Free Jet Turbulent Structure and Impingement Heat Transfer. J. Fluid Mech., vol. 45, pt. 3, Feb. 1971, pp. 477-512.

13. Ames Research Staff: Equations, Tables, and Charts for Compressible Flow. NACA Rep. 1135, 1953.

14. Harsha, Philip T.: Free Turbulent Mixing: A Critical Evaluation of Theory and Experiment. AEDC-TR-71-36, ARO, Inc., 1971.

15. Townsend, A. A.: The Structure of Turbulent Shear Flow. Cambridge University Press, 1956.

16. Hinze, J. O.; and van der Hegge Zijnen, B. G.: Transfer of Heat and Matter in the Turbulent Mixing Zone of an Axially Symmetric Jet. Appl. Sci. Res., vol. A1, no. 5-6, 1949, pp. 435-61.

17. Laurence, James C.: Intensity, Scale, and Spectra of Turbulence in Mixing Region of Free Subsonic Jet. NACA TN 3561, 1955.

18. Hinze, J. O.: Turbulence; an Introduction to its Mechanism and Theory. McGraw-Hill Book Co., Inc., 1959.

19. Bradshaw, P.: An Introduction to Turbulence and its Measurements. Pergamon Press, 1971.

20. Preisser, John S.; and Block, Patricia, J. W.: An Experimental Study of the Aeroacoustics of a Subsonic Jet Impinging Normal to a Large Rigid Surface. AIAA Paper No. 76-520, July 1976.

21. Olsen, W. A.; Gutierrez, O. A.; and Dorsch, R. G.: The Effect of Nozzle Inlet Shape, Lip Thickness, and Exit Shape and Size on Subsonic Jet Noises. NASA TM X-68182, 1973.

22. Powell, Alan: Aerodynamic Noise and the Plane Boundary. J. Acoust. Soc. Am., vol. 32, no. 8, Aug. 1960, pp. 982-990.
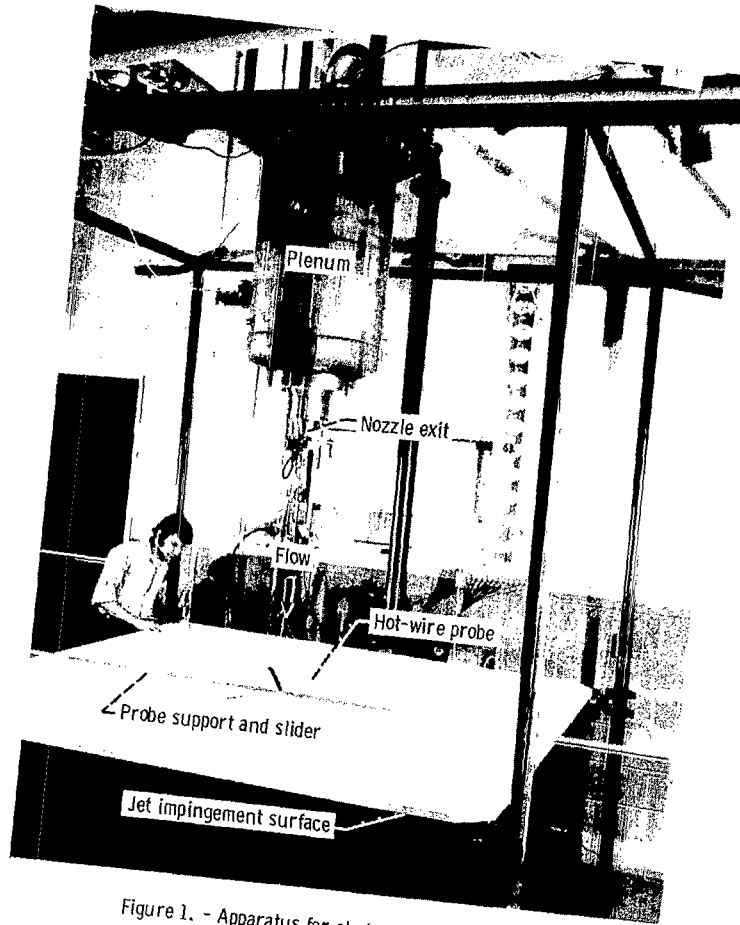
Figure 1. - Apparatus for study of jet impingement.
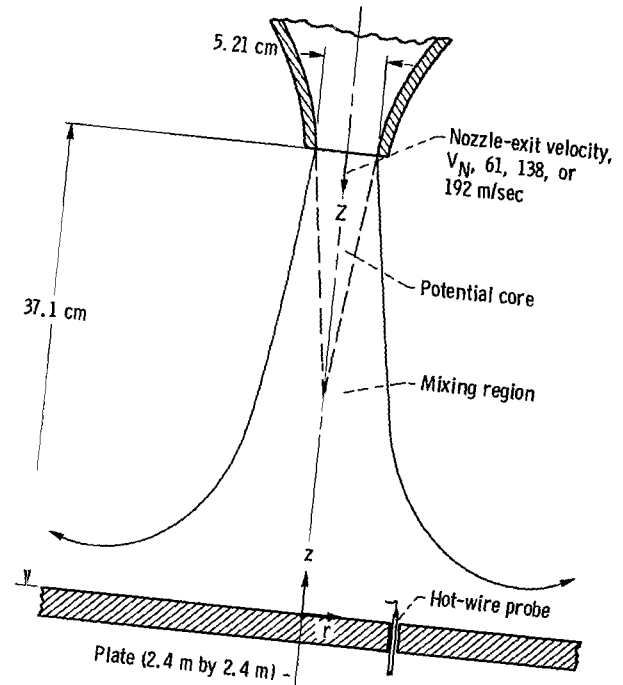
Figure 2. - Free-jet impingement configuration and coordinate system.
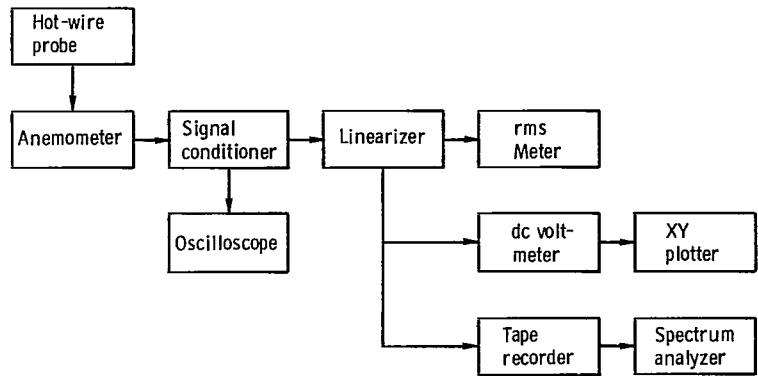
Figure 3. – Schematic of hot-wire measuring system.
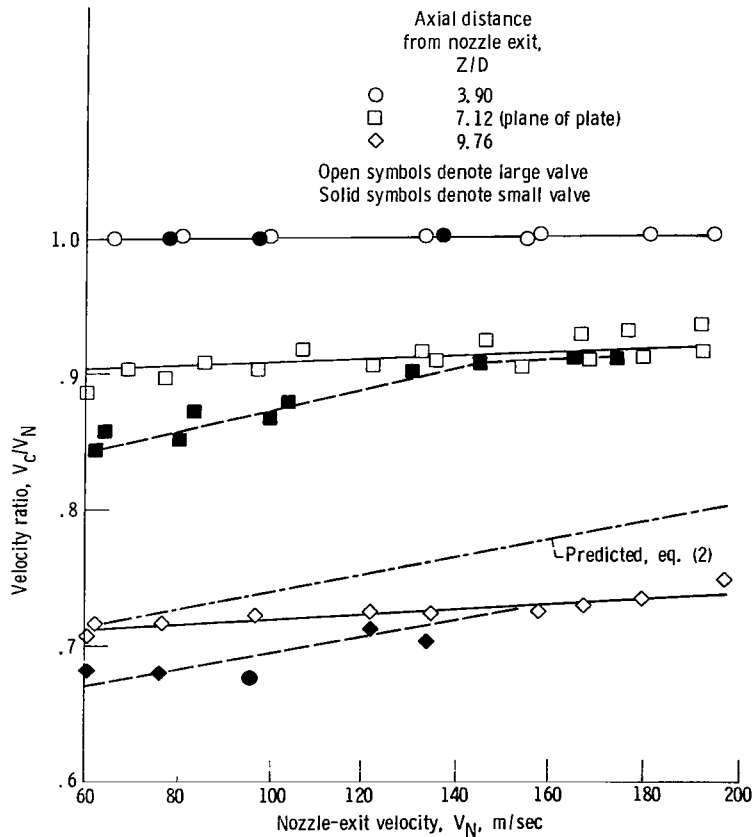
Figure 4. – Variation of free-jet centerline velocity with nozzle-exit velocity for different axial positions. Nozzle diameter, D, 5.21 centimeters.
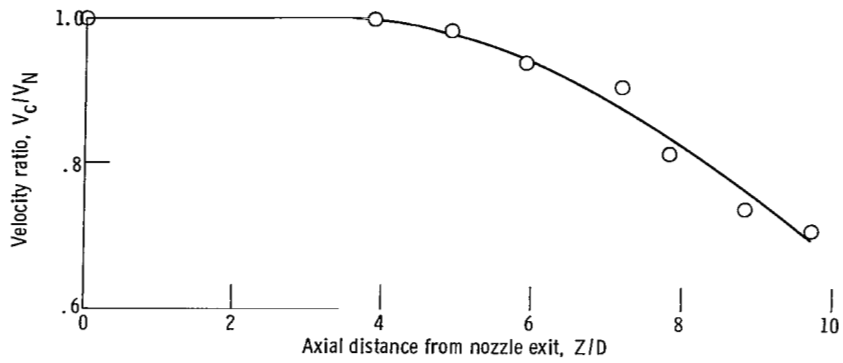
Figure 5. – Variation of free-jet centerline velocity with axial distance from nozzle exit. Nozzle diameter, D, 5.21 centimeters; nozzle-exit velocity, V_N, 138 meters per second.
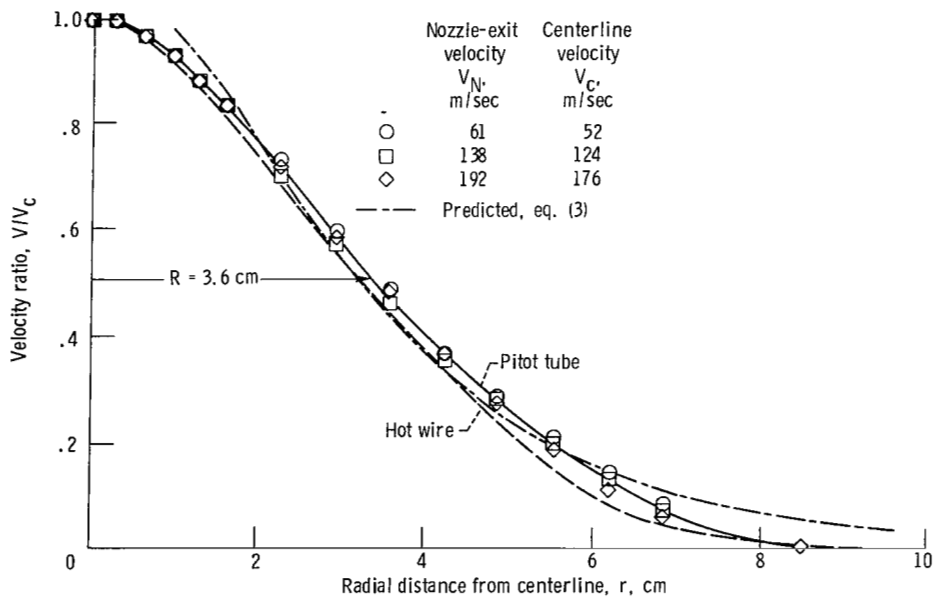
Figure 6. – Free-jet velocity profiles. Axial distance from nozzle exit, Z, 37.1 centimeters.
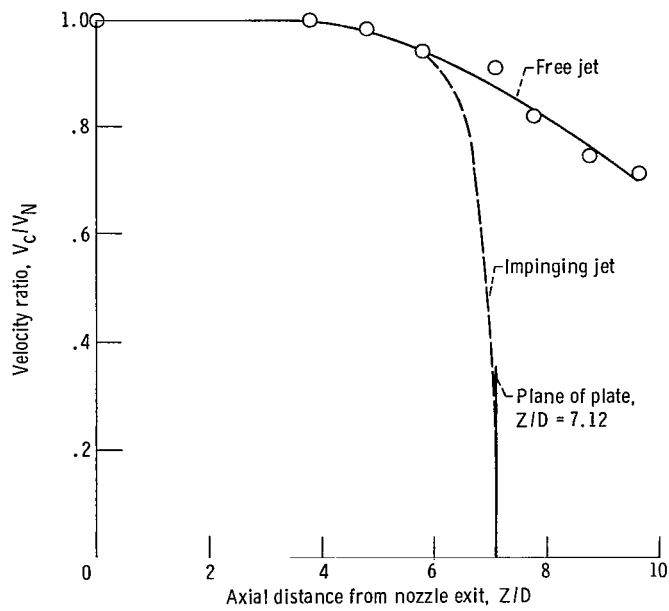
Figure 7. - Variation of centerline velocity with axial distance from
nozzle exit in free and impinging jets. Nozzle diameter, D, 5.21
centimeters; nozzle-exit velocity, V_N, 138 meters per second;
distance between plate and nozzle, 37.1 centimeters.
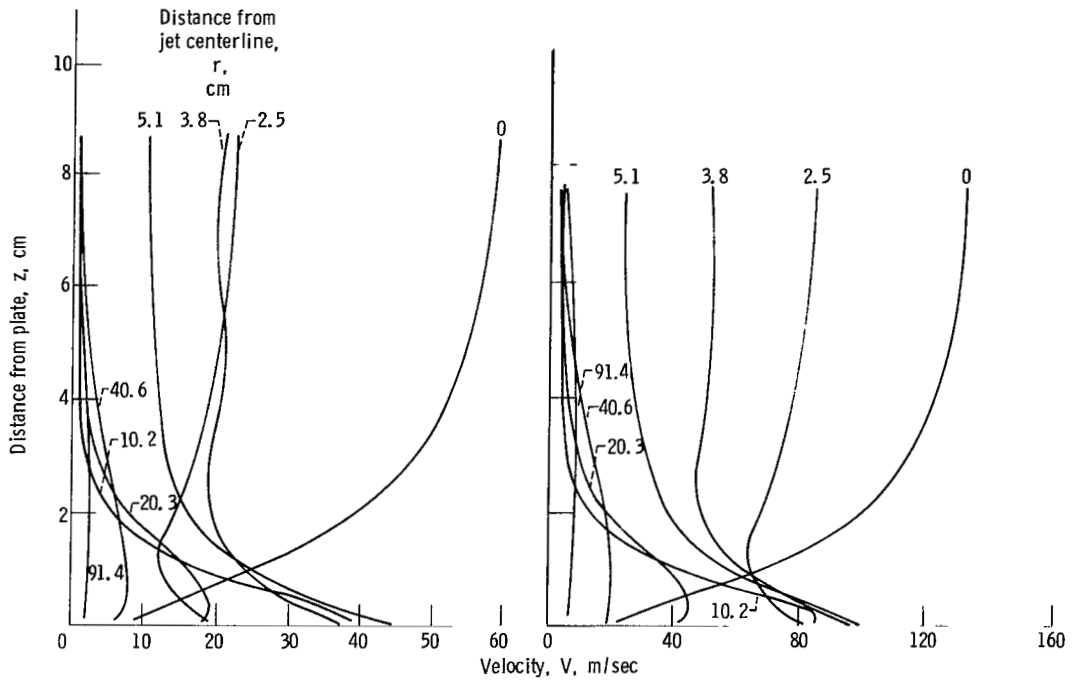
(a) Nozzle-exit velocity, V_N, 61 meters per second.

(b) Nozzle-exit velocity, V_N, 138 meters per second.
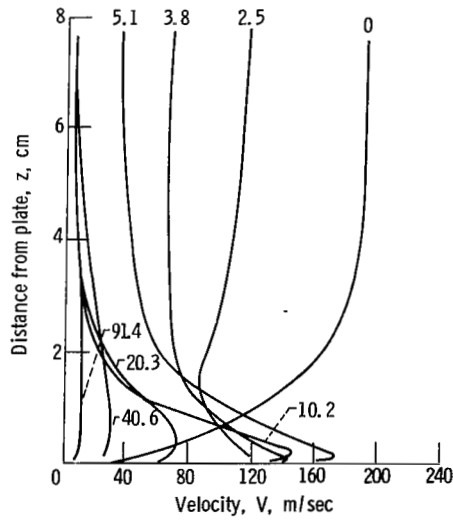
(c) Nozzle-exit velocity, V_N, 192 meters per second.

Figure 8. – Impinging jet velocity profiles in direction of mean flow. Distance between plate and nozzle, 37.1 centimeters.
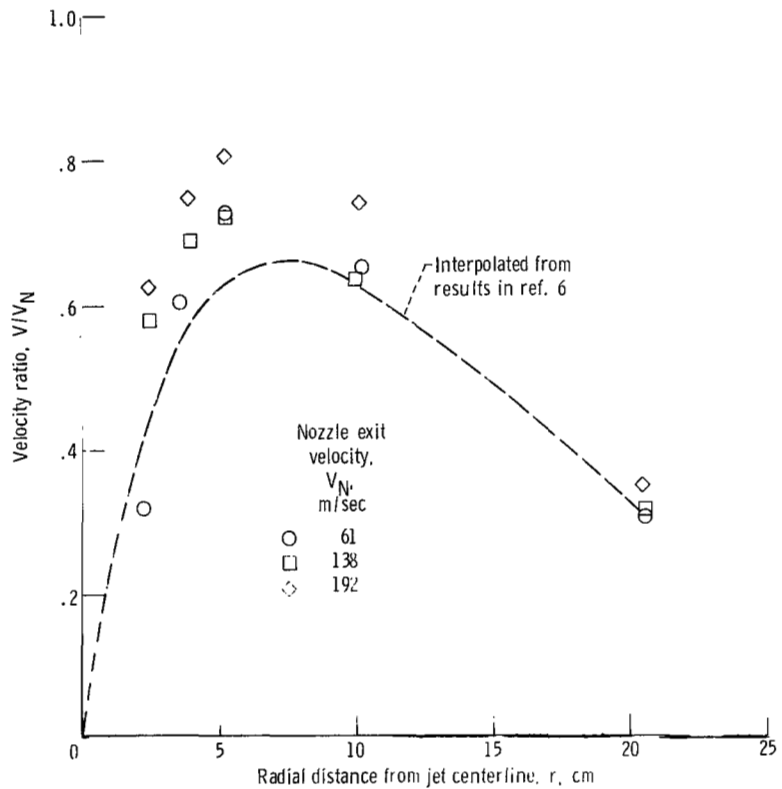
Figure 9. - Distribution of peak velocities near wall in impinging jet. Distance between plate and nozzle, 37.1 centimeters.
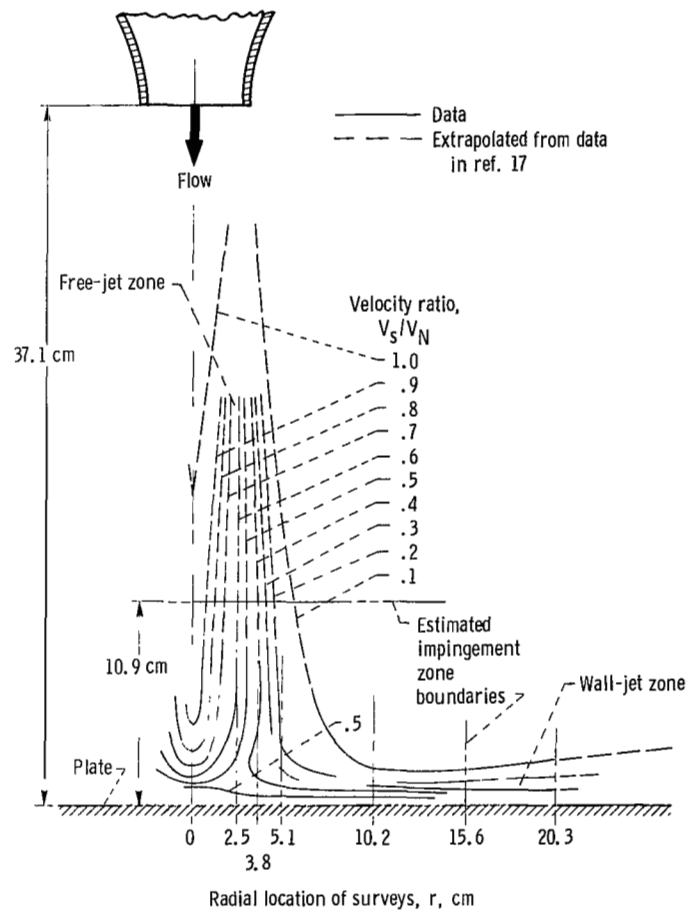
Figure 10. - Contours of constant velocity in impinging flow. Nozzle-exit velocity, V_N, 138 meters per second.
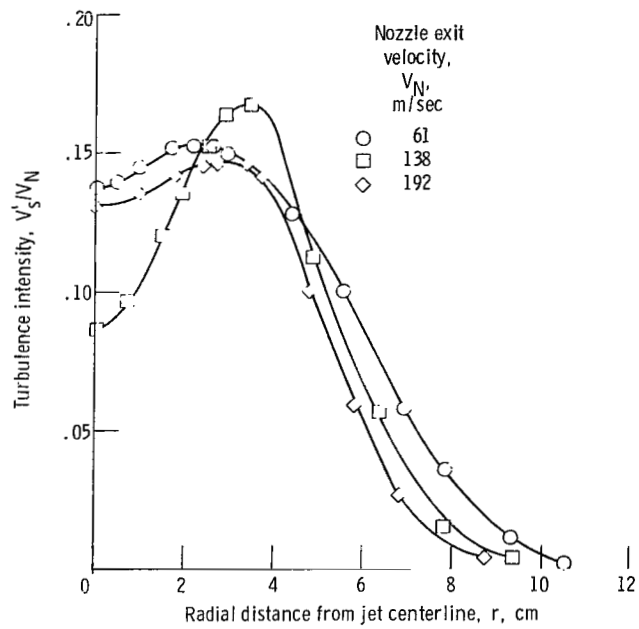
Figure 11. – Turbulence intensity in free jet. Axial distance from nozzle exit, Z, 37.1 centimeters.
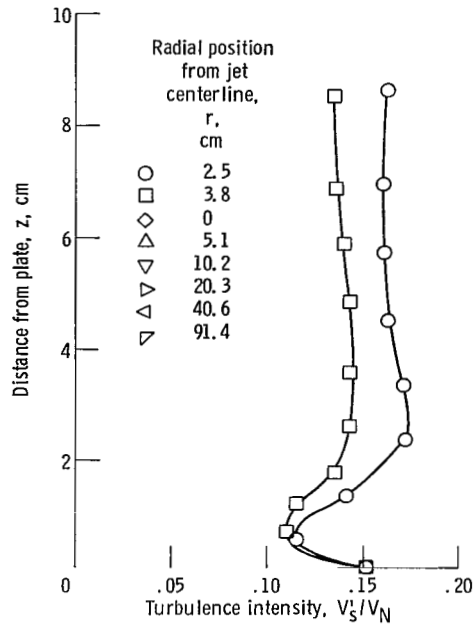
Radial position
from jet
centerline,
r,
cm

○	2.5
□	3.8
◇	0
△	5.1
▽	10.2
▷	20.3
◁	40.6
▽	91.4

(a) Nozzle-exit velocity, V_N, 61 meters per second.

(b) Nozzle-exit velocity, V_N, 138 meters per second.

(c) Nozzle-exit velocity, V_N, 192 meters per second.

Figure 12. - Turbulence intensity in impinging flow. Distance between plate and nozzle, 37.1 centimeters.

27
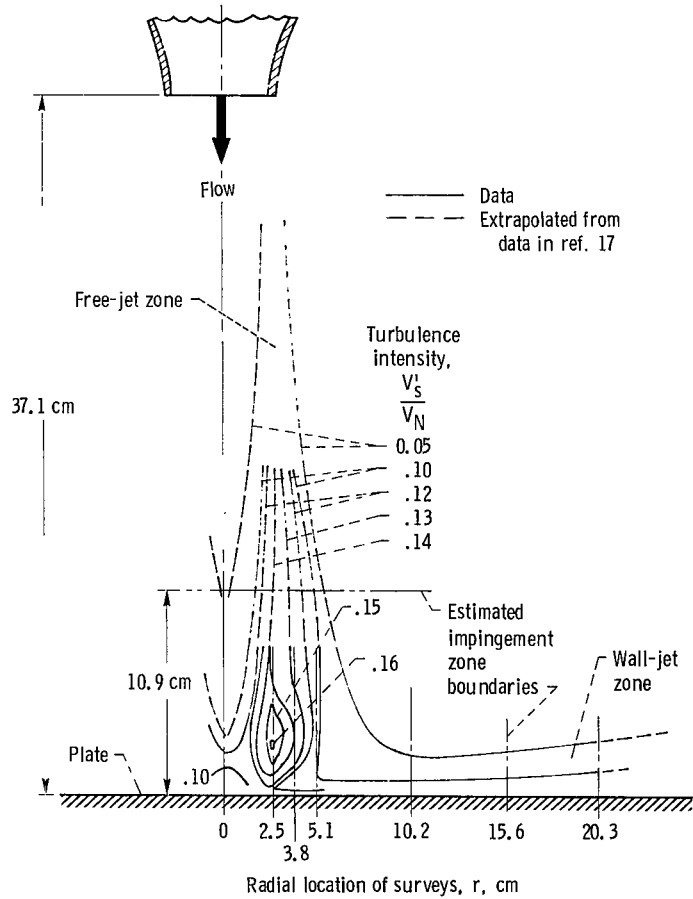
Figure 13. - Contours of constant turbulence intensity in impinging flow. Nozzle-exit velocity, V_N, 138 meters per second.
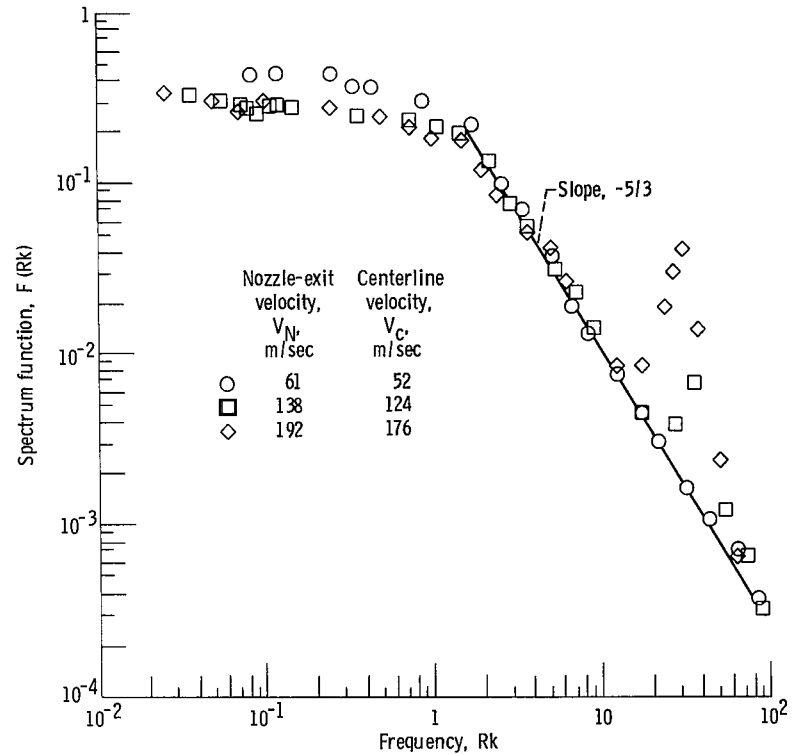
Figure 14. - Spectra of mean-square component of velocity $V_s'^2$ at centerline of free jet. Axial distance from nozzle exit, Z, 37.1 centimeters; reference length, R, 3.6 centimeters.
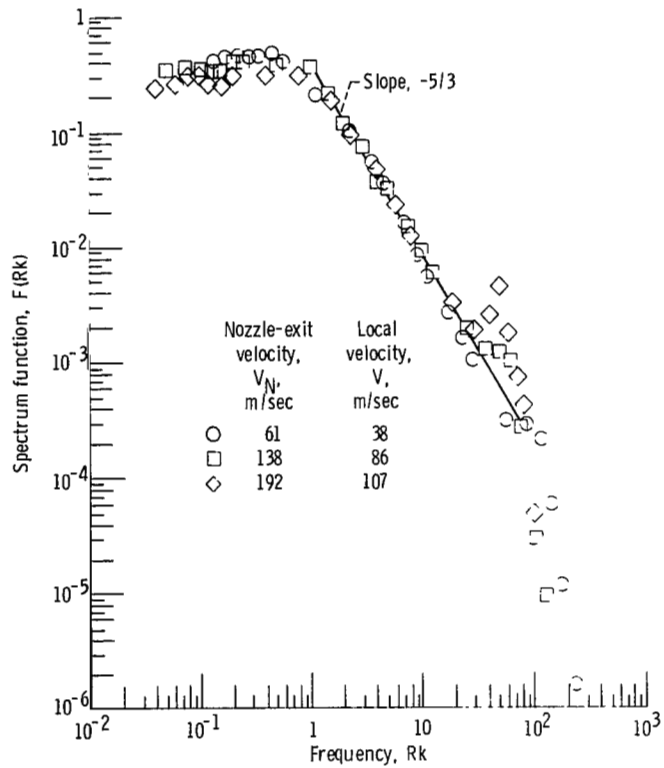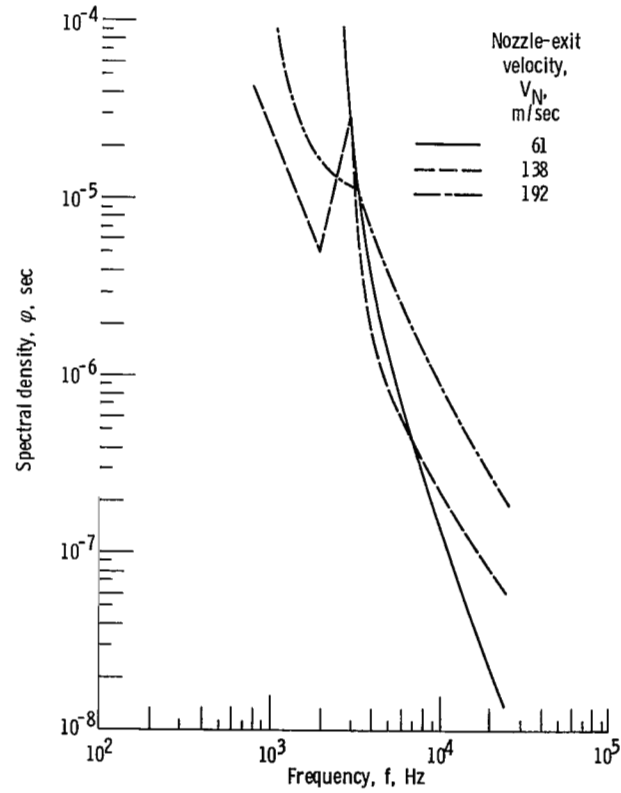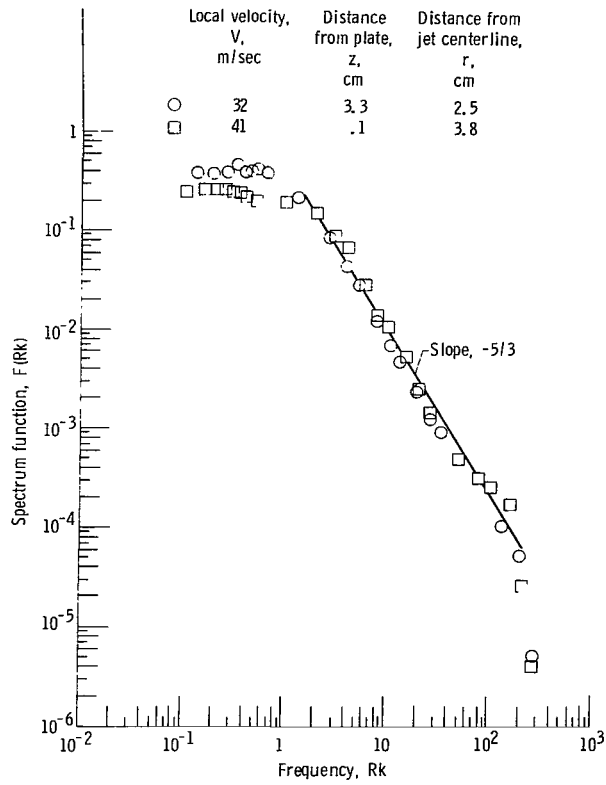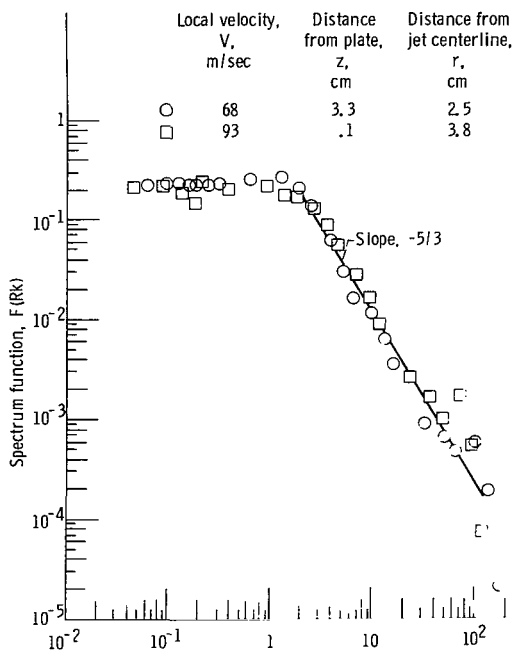
Figure 15. – Spectra of mean-square component of velocity $V_s'^2$ at location of maximum turbulence in free jet. Axial distance from nozzle exit, Z, 37.1 centimeters; reference length, R, 3.6 centimeters.
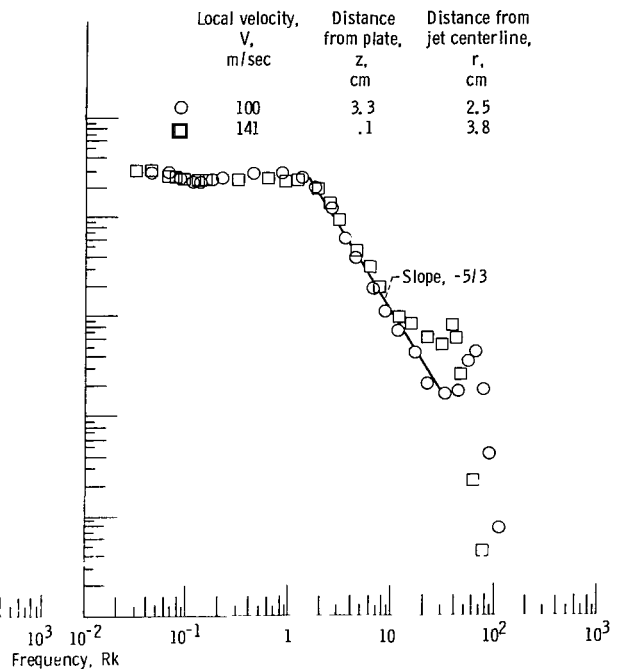

Figure 16. – Narrow-band spectra from a microphone placed outside mixing region of free jet. Distance from nozzle, Z, 36 centimeters; distance from jet centerline, r, 13 centimeters.

Figure 17. - Spectra of mean-square component of velocity V'^2_s at locations of maximum turbulence in impinging flow. Distance between plate and nozzle, 37.1 centimeters; reference length, R, 3.6 centimeters.
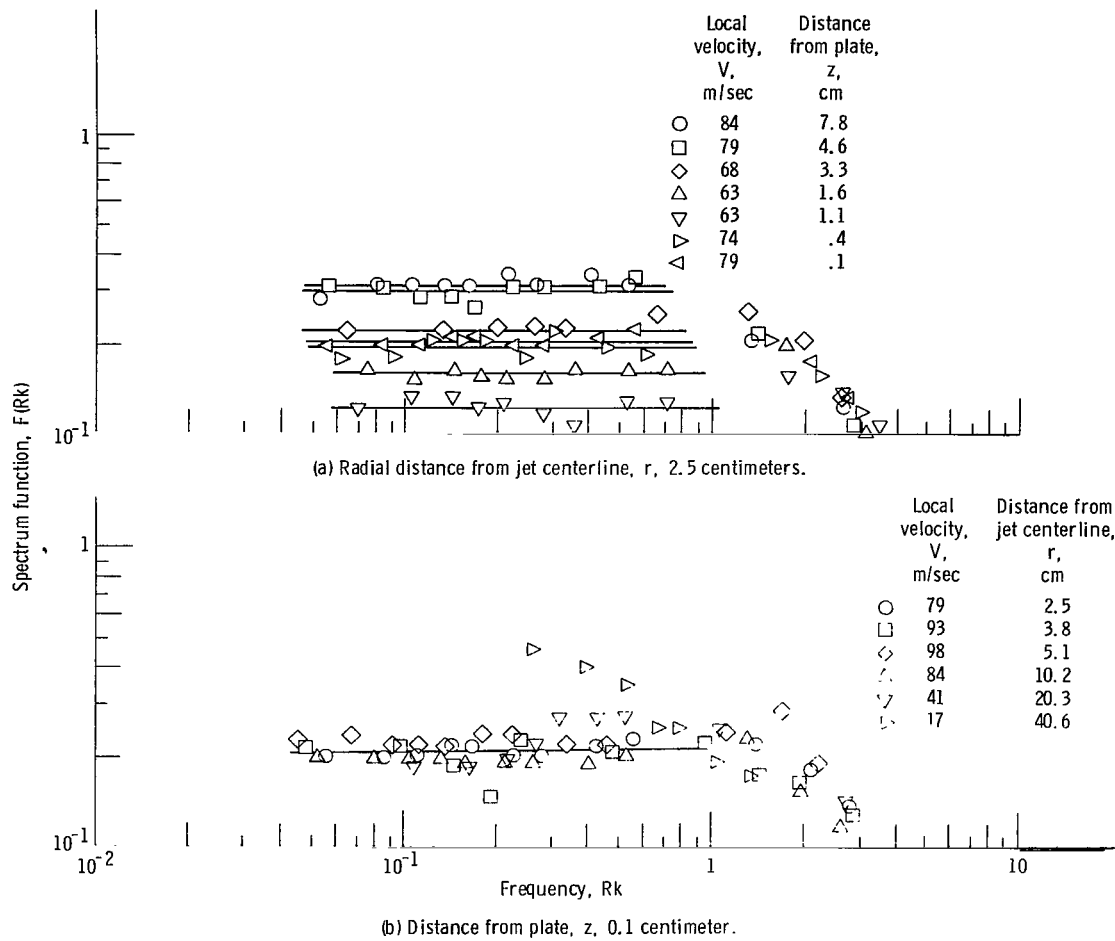
	Local velocity, V, m/sec	Distance from plate, z, cm
○	84	7.8
□	79	4.6
◇	68	3.3
△	63	1.6
▽	63	1.1
▷	74	.4
◁	79	.1

(a) Radial distance from jet centerline, r, 2.5 centimeters.

	Local velocity, V, m/sec	Distance from jet centerline, r, cm
○	79	2.5
□	93	3.8
◇	98	5.1
△	84	10.2
▽	41	20.3
◁	17	40.6

(b) Distance from plate, z, 0.1 centimeter.

Figure 18. – Low-frequency spectra of mean-square component of velocity $V_s'^2$ in impinging flow. Distance between plate and nozzle, 37.1 centimeters; reference length, R, 3.6 centimeters; nozzle-exit velocity, V_N, 138 meters per second.
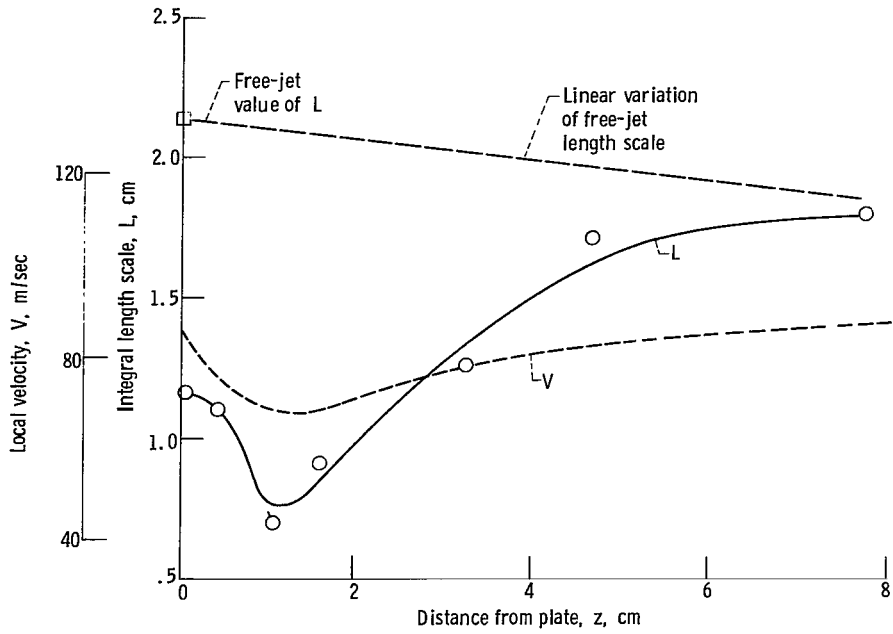
Figure 19. - Integral length scale distribution normal to plate. Distance between plate and nozzle, 37.1 centimeters; nozzle-exit velocity, V_N, 138 meters per second; distance from jet centerline, r, 2.5 centimeters.
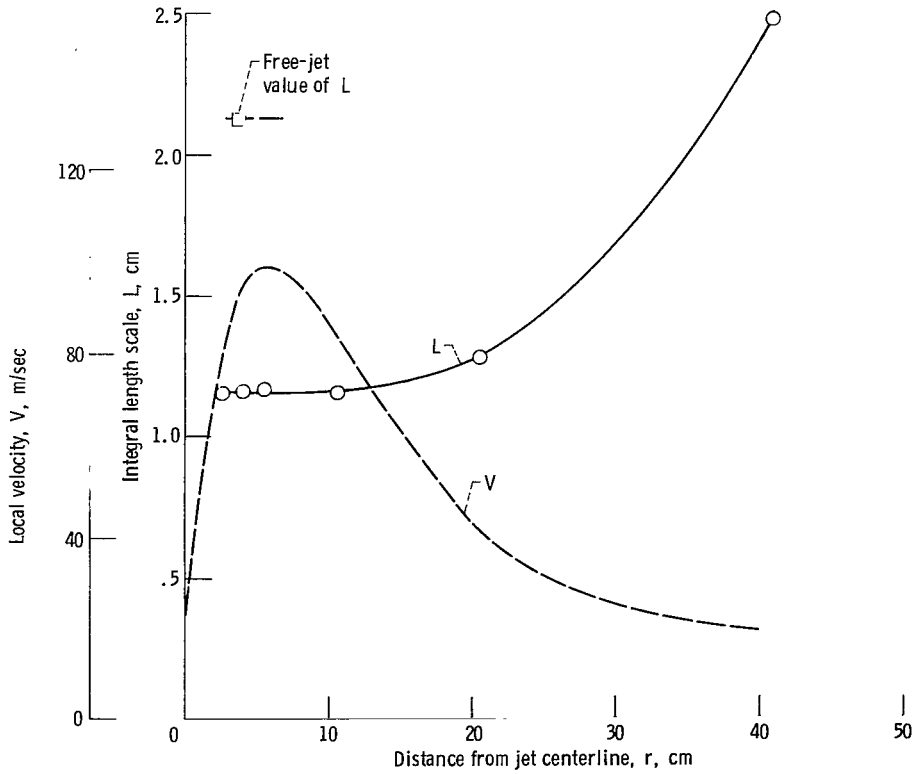

Figure 20. - Integral length scale distribution along plate. Distance between plate and nozzle, 37.1 centimeters; nozzle-exit velocity, V_N, 138 meters per second; distance from plate, z, 0.1 centimeter.
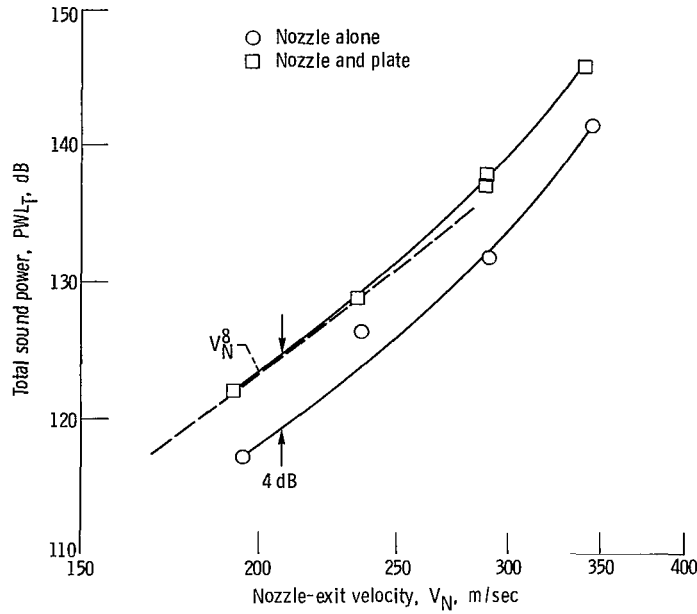
Figure 21. – Variation of sound power level with jet velocity. Nozzle diameter, D, 5.21 centimeters; distance between plate and nozzle, 37.1 centimeters. (Data from ref. 1.)
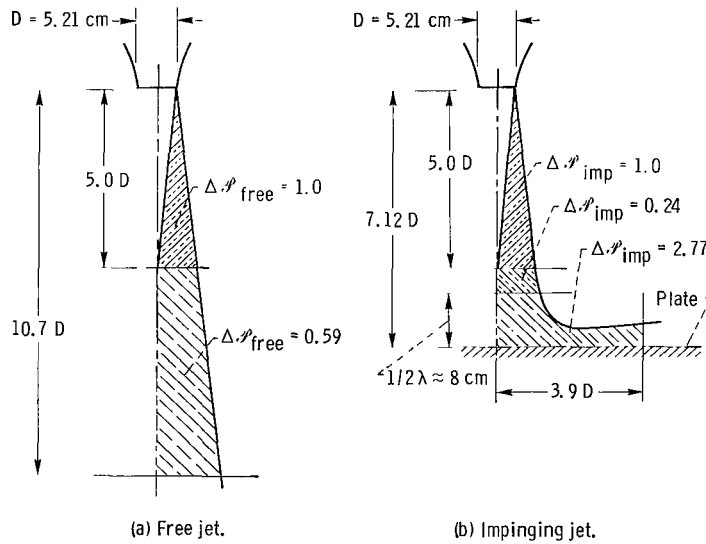

(a) Free jet.   (b) Impinging jet.

Figure 22. – Relative contributions to sound power (eq. (9)) from various regions in free and impinging jets.

1. Report No. NASA TP-1037	2. Government Accession No.	3. Recipient's Catalog No.
4. Title and Subtitle MEAN VELOCITY, TURBULENCE INTENSITY, AND SCALE IN A SUBSONIC TURBULENT JET IMPINGING NORMAL TO A LARGE FLAT PLATE		5. Report Date September 1977
		6. Performing Organization Code
7. Author(s) Donald R. Boldman and Paul F. Brinich		8. Performing Organization Report No. E-8998
		10. Work Unit No. 505-03
9. Performing Organization Name and Address National Aeronautics and Space Administration Lewis Research Center Cleveland, Ohio 44135		11. Contract or Grant No.
		13. Type of Report and Period Covered Technical Paper
12. Sponsoring Agency Name and Address National Aeronautics and Space Administration Washington, D. C. 20546		14. Sponsoring Agency Code

15. Supplementary Notes

16. Abstract

To explain the increase in noise when a jet impinges on a large flat plate, mean velocity, turbulence intensity, and scale were measured at nominal nozzle-exit velocities of 61, 138, and 192 meters per second with the plate located 7.1 nozzle-exit diameters from the nozzle. The maximum turbulence intensities in free and impinging jets were about the same; however, the integral length scale near the plate surface was only about one-half the free-jet scale. The measured intensities and length scales, in conjunction with a contemporary theory of aerodynamic noise, provided a good explanation for the observed increase in noise associated with the impinging jet. An increase in the volume of highly turbulent flow could be the principal reason for the increase in noise.

17. Key Words (Suggested by Author(s)) Fluid mechanics Aerodynamics Acoustics	18. Distribution Statement Unclassified - unlimited STAR Category 34		
19. Security Classif. (of this report) Unclassified	20. Security Classif. (of this page) Unclassified	21. No. of Pages 34	22. Price* A03